Progress In Electromagnetics Research, Vol. 126, 481–497, 2012

ADAPTIVE SAMPLING IN MULTILEVEL PLANE WAVE BASED NEAR-FIELD FAR-FIELD TRANSFORMED PLANAR NEAR-FIELD MEASUREMENTS

M. A. Qureshi*, C. H. Schmidt, and T. F. Eibert

Technische Universität München, Lehrstuhl für Hochfrequenztechnik, 80290 Munich, Germany

Abstract—An adaptive approach to minimize acquisition time in planar near-field antenna measurements is described. In contrast to the traditional planar near-field scanning, the presented technique acquires the near-field in form of rectangular rings and skips sampling points in smoothly varying near-field regions. Abrupt changes in the near-field are detected by comparing extrapolated and measured near-field values at coarser sampling points. A decision function based on the signal-to-noise ratio (SNR) of the measured value is used to determine the threshold difference between the measured and the extrapolated near-field values for skipping the sampling point. Near-field data thus collected on the resultant irregular grid is processed using the multilevel plane wave based near-field far-field transformation algorithm. The multilevel transformation algorithm is computationally efficient and capable of handling data collected on irregular grids. A rigorous analysis of the adaptive data acquisition approach is then performed in terms of transformed far-field accuracy, decision factor, and test time reduction. Several test cases covering a variety of antennas are shown using synthetic as well as measured data for realistic results. Afterwards the acquisition time for the worst case scenario is compared with the traditional planar near-field measurement technique.

1. INTRODUCTION

The radiation pattern of an antenna under test (AUT) can be characterized by determining the radiating near-field on a spherical [1], cylindrical [2], planar [3], or any other arbitrary surface [4, 5] and processing the acquired near-field using a near-field far-field (NFFF)

Received 8 February 2012, Accepted 8 March 2012, Scheduled 2 April 2012

* Corresponding author: Muhammad Ayyaz Qureshi (ayyaz.qureshi@mytum.de).

transformation algorithm [6]. Near-field antenna measurements provide a suitable alternative to expensive compact ranges and space-limited far-field measurements for large antennas. However, the accuracy of the transformed patterns is greatly dependent on the accuracy of the near-field along with the suitable transformation algorithm.

Planar near-field (PNF) antenna measurements are appropriate for medium and high gain antennas and ideally require measurements on an infinite plane. Reducing the scan plane size, due to practical limitations, reduces the reliable region of the far-field pattern and also introduces truncation errors within the reliable region [7]. On the other side, increasing the scan plane size would directly result in an increased testing time. Several methods have been proposed in the recent past to cope with the truncation effects. This would allow a larger reliable region while keeping the smaller scan size, hence reducing the measurement time. One method [8] uses a set of equivalent magnetic currents over a fictitious planar surface to characterize the antenna. The near-field is related to the equivalent magnetic currents using integral equation. This method provides a larger reliable region as compared to modal expansion methods in which radiated antenna fields are expanded in terms of planar wave functions [9]. As stated by the author, the method is not suitable for highly directive antennas [8] dissolving the major benefit of PNF measurements. Another method in [10] utilizes *a priori* information, i.e., the size of the antenna and "recovers" the lost information content due to the area truncation by employing the sampling theory. However, the effectiveness of this method depends on the fact that the probe can also move in a direction perpendicular to the measurement plane which eventually increases measurement time. The Gerchberg-Papoulis iterative algorithm is applied in [12] to extrapolate the plane wave spectrum of the field radiated by the antenna to overcome the truncation problem. Back-projections and re-adjustments are recursively applied to the originally determined plane wave spectrum until the given convergence criterion is met. This method of projections is prone to so-called traps and tunnels and may not converge [11]. In another approach in [15], the near-field data is extrapolated outside the measurement region by employing the optimal sampling interpolation (OSI) expansions instead of cardinal series (CS) ones. The comparison between OSI and CS based approach is performed afterwards using numerical simulations and significant enlargement of the valid far-field region is reported. A similar non-redundant sampling representation in electromagnetic field based approach is applied in bipolar scanning for extrapolating near-field values outside the measurement plane in [17]. The external data is estimated by employing singular value decomposition method

and using OSI expansions. Significant decrease in the truncation error occuring in near-field far-field transformation is reported for bipolar scanning.

An effective planar spiral scanning technique described in [14] utilizes ellipsoidal modelling of the source [13] instead of the spherical one. The said technique gives the freedom of considering measurement plane at distances smaller than one half of the antenna size, and therefore increases the valid angle associated with the size of the scan plane for quasi-planar antennas. The technique works well as long as the decreased separation does not increase the multiple reflections between the AUT and the probe. The planar wide-mesh scanning is applied in [16] with sample spacing greater than half-wavelength when moving away from the center of the scanning region. The amount of required near-field data is significantly reduced without decreasing the accuracy and no drastic change is required in existing plane-rectangular facility. Although the number of sampling points are reduced but the effect on the acquisition time is not reported.

Recently, an adaptive acquisition technique has been proposed in [18] to reduce the measurement time by rectangular spiral scanning of the probe. It considerably reduces the measurement time by terminating the measurement process when a specific accuracy is reached dependent on a decision factor. The decision factor, as explained in [18], is based on either the first side lobe level pattern difference or the directivity of the given AUT. It is shown that considerable decrease in the acquisition time can be achieved if the measurement process is terminated optimally. Nevertheless, if the measurement is terminated at a smaller scan plane size the reliable region is also reduced accordingly. Also, NFFF transformations after each rectangular ring acquisition make it difficult to use transformation algorithms employing integral equations which usually require long computation times.

In this paper, we present a simple approach to reduce the measurement time in PNF measurements. In contrast to the adaptive acquisition in [18], the valid angle is not reduced and as such no extra measurement step is required. The measurement system adapts itself during the measurement process and based on a given decision threshold, it concentrates mainly on the strongly changing near-field regions while skipping data points from smoothly varying locations. However, the extent at which the measurement time is reduced depends on the near-field distribution. Best results have been achieved for antennas with smoothly varying near-fields. The irregular grid obtained as a result of adaptive scanning is processed using the multilevel plane wave based NFFF transformation algorithm. We

already showed earlier in [19] that the multilevel technique is more robust against truncation error as compared to conventional two dimensional Fast Fourier Transform (2DFFT) based approaches and that it is suitable for electrically large antennas [20]. Furthermore, full probe correction is accomplished without increase in complexity [20].

In Section 1, the adaptive approach used to acquire the near-field in planar measurements along with composition of the decision factor is described. The multilevel plane wave based NFFF transformation algorithm is revisited in Section 2. Finally in Section 3, the performance of the adaptive approach is evaluated for a variety of antennas using both synthetic and measured data for realistic results. Data generation for synthetic data is also explained in the same section.

2. ADAPTIVE PLANAR NEAR-FIELD MEASUREMENT

2.1. General Formulation

The boundaries of the scan plane in the PNF measurement are defined by selecting a valid angle for the reliable region of interest. A simple relation

$$\Theta_{\text{valid}} \simeq \tan^{-1}\left(\frac{L-d}{2s}\right) \tag{1}$$

involving length of the square shaped scan plane L, aperture size of the AUT d, and measurement distance s, has been developed from extensive measurements [22] and is derived from theoretical analysis [21]. The size of the scan plane is usually chosen to provide less than $-35\,\text{dB}$ truncation level at the edges for minimum error in the valid region. In the traditional approach, data acquisition from the defined area is achieved by linear motion of the probe in the vertical direction while stepping in the horizontal or vice versa (as shown in Fig. 2 of [18]).

We recognize that the distribution of the near-field on the measurement plane is of prime importance containing more information contents in suddenly changing regions compared to smoothly varying locations within the scan plane. Therefore, avoiding data points from smooth areas and thereby saving measurement time will have a negligible effect on the radiation pattern of the AUT. To determine sudden variations during the measurement process, we propose a ring shaped data acquisition approach. The data acquisition starts from the center of the scan plane and steps in the outward direction away from the center. In the beginning, near-field acquisition starts from the center of the scan plane and the main beam data

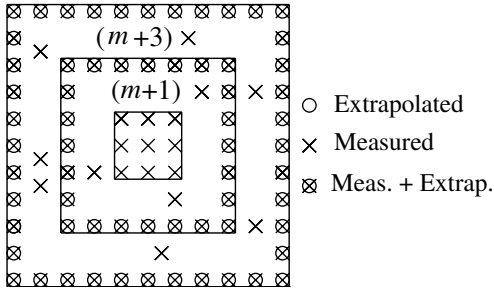

Figure 1. Measurement plane dividing sampling points into rectangular rings. Depending on difference in the extrapolated and the measured values of $(m+2)$ ring points, selected points have been measured in $(m+1)$ ring.

is obtained until the mth ring[†]. Using the acquired data, we then extrapolate near-field values $\mathbf{U}_{\text{ext}}^{(m+2)}$ at the measurement points of the $(m+2)$ ring while skipping the $(m+1)$ ring. Afterwards, sampling points of $(m+2)$ ring are measured providing $\mathbf{U}_{\text{meas}}^{(m+2)}$. The logarithmic differences between the extrapolated and the measured values

$$\mathbf{D}^{(m+2)} = 20\log_{10}\left(\text{abs}\left(\mathbf{U}_{\text{ext}}^{(m+2)} - \mathbf{U}_{\text{meas}}^{(m+2)}\right)\right) \tag{2}$$

determine whether the corresponding points from the $(m+1)$ ring can be skipped or not. The list containing sampling points is constantly updated and once the probe finishes traversing the $(m+2)$ ring, it steps back to the $(m+1)$ ring and measures only the non-skipped points. It is worth mentioning here that extrapolated near-field values are only used to locate the unexpected change in the near-field and are not used in the NFFF transformation itself so any standard extrapolation technique can serve the purpose. We utilize Piecewise Cubic Hermite Interpolation (pchip) to extrapolate out of range values. Fig. 1 shows a measurement plane divided into a rectangular ring structure.

2.2. Decision Criterion

A suitable choice of decision criterion will determine the threshold difference $D_{\text{th}}^{(m+2)}$ for skipping the data point. Obviously, one cannot use a fixed value for all the data points as it should vary with the

[†] It is assumed here for simplicity that the main beam lies in the center of the scan plane. However, if the main beam does not lie in the center or the exact location of the main beam is not known, data acquisition can be started from any other part of the scan plane provided that the main beam would lie in that specific portion acquired in the beginning.

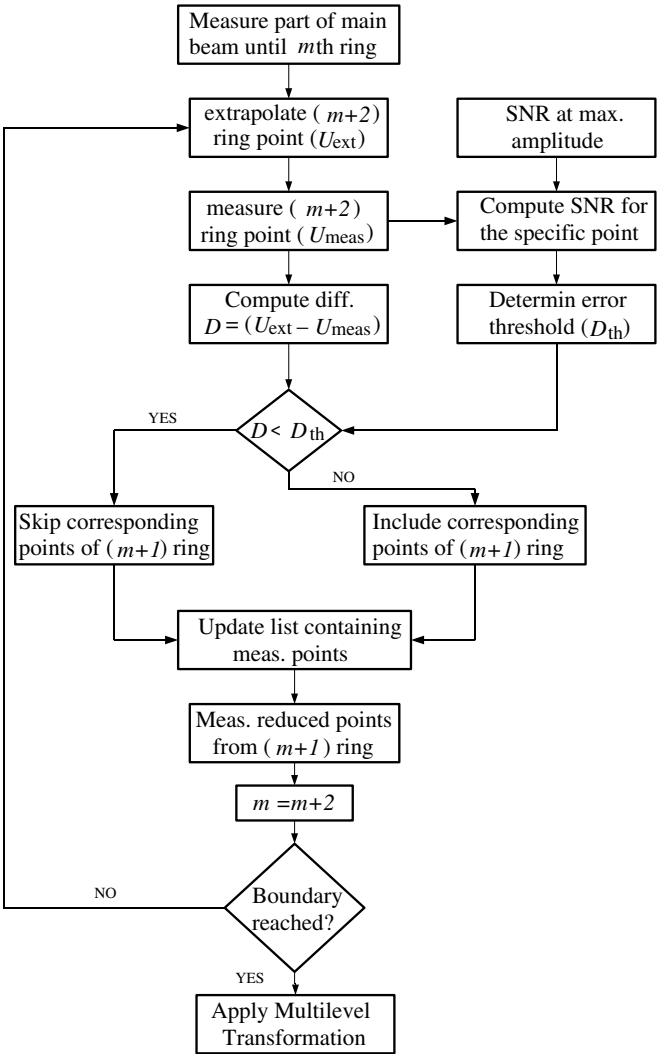

Figure 2. Schematic of the proposed procedure.

near-field magnitude for reliable results. We introduce a unique way to define the decision criterion based on signal-to-noise ratio (SNR) of the received signal. An SNR of 60 dB‡ (can be varied) is assumed at the maximum pattern level and is decreased down to 30 dB at 30 dB below the maximum pattern level. The intermediate points can be linearly

‡ The SNR value is deduced empirically from practical measurements.

interpolated and the threshold difference is empirically computed as

$$D_{\text{th}}^{(m+2)} = 20\log_{10}\left(\frac{1}{3}\left(1+\sqrt{\frac{0.5}{10^{\frac{\text{SNR}}{10}}}}\right)\right). \tag{3}$$

Afterwards, the threshold difference is compared with the computed difference as

$$D^{(m+2)} - D_{\text{th}}^{(m+2)} = \begin{cases} < 0 & \text{skip point} \\ \geq 0 & \text{include point} \end{cases} \tag{4}$$

and the corresponding points from ring $(m+1)$ are skipped according to the given condition. Fig. 2 shows the schematic of the designed algorithm. The process is recursively repeated until the boundary of the scan plane is reached when it terminates. The given procedure is equally valid for square as well as rectangular grids. The only difference occurs in acquiring the initial data from the center which is in accordance with the shape of the grid.

2.3. Multilevel Near-field Transformation

An irregular planar grid data with non-uniform spacing between the sample points is obtained by using the adaptive approach explained in Section 2.1. The classical technique employing modal expansion of plane wave functions can only handle the data collected on a regular grid. We apply the multilevel plane wave based NFFF transformation which is suitable for irregular grids. The multilevel technique has a low computational complexity and full probe correction can also be achieved without increase in the complexity. It has already been validated using simulation as well as experimental results [5, 20]. Additionally, robustness against scan area truncation is observed as compared to traditional techniques employing 2D FFT [19]. In this section, we review the fundamentals of this technique.

The field probe takes the weighted average of the field strength around the measurement point together with the receiving characteristics of the probe and the output signal

$$U\left(\mathbf{r}_{\text{M}}\right) = \iiint\limits_{V_{\text{probe}}} \mathbf{w}_{\text{probe}}\left(\mathbf{r}\right) \cdot \mathbf{E}\left(\mathbf{r}\right) dV \tag{5}$$

is acquired at the measurement point $\mathbf{r}_{\text{M}}$. V_{probe} is the volume and $\mathbf{w}_{\text{probe}}$ contains the spatial weighting function of the probe. The multilevel technique uses plane waves $\left(\bar{\mathbf{I}} - \hat{k}\hat{k}\right) \cdot \tilde{\mathbf{J}}\left(\hat{k}\right)$ as equivalent sources to reconstruct the radiated fields of the AUT as shown in Fig. 1 of [19]. Unlike the classical plane wave based approach, the

multilevel technique utilizes the complete Ewald sphere of propagating plane waves and relates the plane wave spectrum and near-field samples using the diagonal translation operator $T_L\left(\hat{k}, \hat{r}_{\mathrm{M}}\right)$ (known from Fast Multipole Method [23]) according to

$$\mathbf{U}\left(\mathbf{r}_{\mathrm{M}}\right) = -\mathrm{j}\frac{w\mu}{4\pi}\oiint T_L\left(\hat{k}, \hat{r}_{\mathrm{M}}\right)\bar{\mathbf{P}}\left(\hat{k}, \hat{r}_{\mathrm{M}}\right)\cdot\left(\bar{\mathbf{I}} - \hat{k}\hat{k}\right)\cdot\tilde{\mathbf{J}}\left(\hat{k}\right)d\hat{k}^2 \tag{6}$$

where $\bar{\mathbf{P}}\left(\hat{k}, \hat{r}_{\mathrm{M}}\right)$ contains the far-field pattern of the probe for probe correction. For optimum computational complexity, measurement points are grouped together to form a hierarchical structure similar to Multilevel Fast Multipole Method (MLFMM). Fig. 3 shows cross-section of the multilevel scheme with cubical box structure. In contrast to the single level case, field translations can now be carried out on the coarsest level. The plane wave spectra

$$\tilde{\mathbf{J}}_N^{i_N}\left(\hat{k}\right) = T_L\left(\hat{k}, \hat{r}_{\mathrm{box}}\right)\left(\bar{\mathbf{I}} - \hat{k}\hat{k}\right)\cdot\tilde{\mathbf{J}}\left(\hat{k}\right) \tag{7}$$

are received at the boxes on the coarsest level i_{N}. Recursive disaggregation and anterpolation is then performed to process the plane wave spectra from coarsest to the finer level box centers according to

$$\tilde{\mathbf{J}}_n^{i_n}\left(\hat{k}\right) = \bar{\mathbf{D}}_n^{i_n}\left(\mathbf{k}, \mathbf{r}_n^{i_n}\right)\cdot\left(\bar{\mathbf{I}} - \hat{k}\hat{k}\right)\cdot\tilde{\mathbf{J}}_{n+1}^{i_{n+1}}\left(\hat{k}\right) \tag{8}$$

using the combined disaggregation and anterpolation operator $\bar{\mathbf{D}}_n^{i_n}\left(\mathbf{k}, \mathbf{r}_n^{i_n}\right)$. Disaggregation simply reflects phase shift from the parent to the child box centers and finally to the measurement points while anterpolation is a way of reducing the sampling rate from a higher to a lower value, thus reducing the overall complexity. More details about the said operator can be found in [20]. Once the anterpolation and

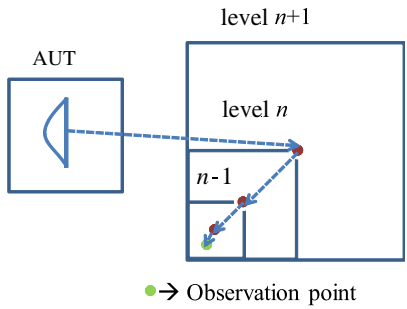

Figure 3. Multilevel measurement setup.

disaggregation is completed, the probe output signal

$$\mathbf{U}(\mathbf{r}_{\mathrm{M}}) = -\mathrm{j}\frac{w\mu}{4\pi}\sum_{\hat{k}}\mathbf{W}\left(\hat{k}\right)\mathrm{e}^{-\mathrm{j}\tilde{\mathbf{r}}_{\mathrm{M}}\cdot\mathbf{k}}\bar{\mathbf{P}}\left(\hat{k},\hat{r}_{\mathrm{M}}\right)\cdot\left(\bar{\mathbf{I}}-\hat{k}\hat{k}\right)\cdot\tilde{\mathbf{J}}_0^{i_0}\left(\hat{k}\right) \quad (9)$$

is computed by proper weighting the plane waves with their respective probe co-efficients. Gauss-Legendre quadrature is used for evaluation of the integrals and the algorithm is implemented in an iterative manner by using the Generalized Minimum Residual Solver (GMRES) [24].

3. PERFORMANCE EVALUATION

3.1. Near-field Data Acquisition

In order to assess the performance of the proposed procedure, we begin by modeling the AUT using synthetic data. Electric dipoles are used to model the AUT with proper magnitude profile and geometrical arrangement as explained in [25]. A high gain parabolic reflector ($64\,\lambda$) and a medium gain horn ($4\,\lambda$) are designed with source dipoles arranged in concentric circles. The accumulative effect of all the source dipoles determines the electric field

$$\mathbf{E}(\mathbf{r}_{\mathrm{M}}) = -\mathrm{j}\frac{\omega\mu}{4\pi}\sum_{i=1}^{i_{\mathrm{AUT}}}\left(\bar{\mathbf{I}}+\frac{1}{k^2}\nabla\nabla\right)\cdot\mathbf{d}_i\frac{\mathrm{e}^{-\mathrm{j}k\left|\mathbf{r}_{\mathrm{M}}-\mathbf{r}_{\mathrm{d},i}\right|}}{\left|\mathbf{r}_{\mathrm{M}}-\mathbf{r}_{\mathrm{d},i}\right|} \quad (10)$$

at the measurement point $\mathbf{r}_{\mathrm{M}}$ by evaluating the Green's function of free space where $\mathbf{r}_{\mathrm{d},i}$ represents the source dipole positions, ω is the angular

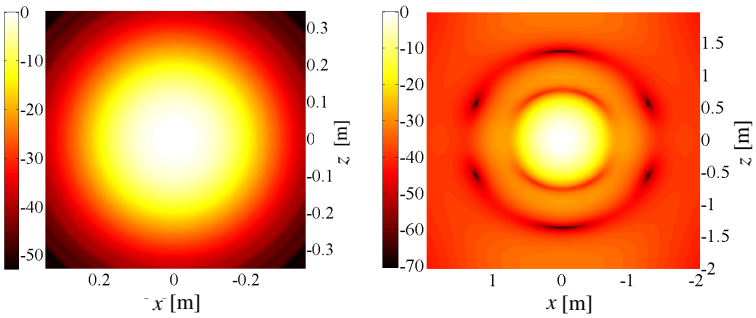

Figure 4. Near-field distribution (dB) of (a) high gain parabolic reflector and (b) medium gain horn operating at 40 GHz and 10 GHz, respectively.

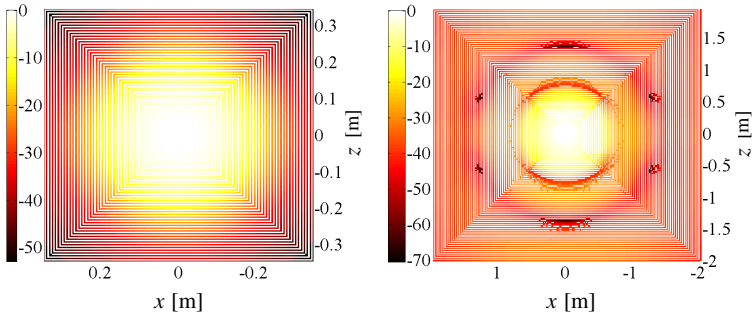

Figure 5. Adaptive near-field acquisition of (a) high gain parabolic reflector and (b) medium gain horn. White rings denote the location of skipped data.

Figure 6. Shaped-beam antenna mounted in an anechoic chamber.

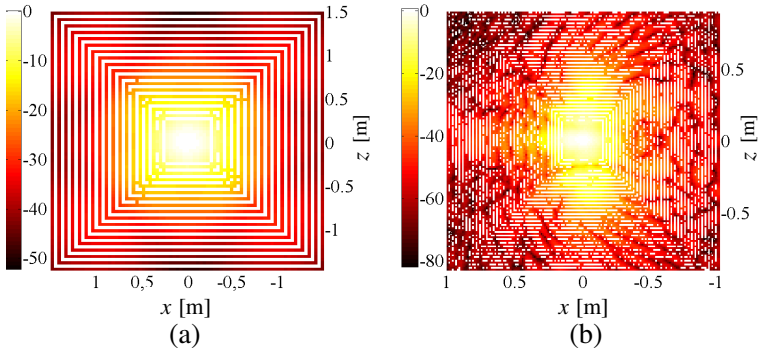

Figure 7. Adaptive near-field acquisition of (a) broad beam and (b) shaped beam antenna. White rings denote the location of skipped data.

frequency, k is the wavenumber of free space, $\bar{\mathbf{I}}$ is the unit dyad, and $\mathbf{d}_i$ represents the amplitude, phase, and polarization information of the source dipoles. The near-field distribution of both antennas collected in the xz-plane and placed at $y = -1.5$ m with half-wavelength sample spacing is shown in Fig. 4. As observed, the near-field of the high gain antenna varies smoothly but the medium gain horn contains fluctuations.

Afterwards, the proposed adaptive approach is applied considering 20 dB SNR at maximum amplitude in the decision threshold and is decreased down accordingly, as explained in Section 2.2. The resulting near-field distribution is shown in Fig. 5. Apart from part of the main beam acquired in the beginning, it can be seen that every alternate near-field ring for the parabolic reflector is skipped making a full-wavelength sample spacing. Sudden changes in the horn near-field distribution are successfully detected at run time, hence data is acquired accordingly. For realistic comparisons, we also use measured data of a broad beam and a shaped beam antenna (see Fig. 6) operating at 4 GHz and 12 GHz, respectively. The proposed procedure is applied to the measurement data and the adaptive near-field distribution is shown in Fig. 7. Significant reduction of data points can be seen in the field distribution of the broad beam antenna while less reduction of data points is observed for the shaped beam antenna.

To get more insight into the effect of changing the SNR in the decision criterion, the SNR is varied from 80 dB to 20 dB at the highest near-field amplitude. On decreasing the SNR the number of measurement points also decreased. However, less reduction of measurement points is observed for the shaped beam antenna due to abrupt changes in the near-field distribution.

3.2. Far-field Accuracy

Adaptive and regular near-field data of both synthetic and real antennas are processed using the multilevel transformation. The transformed far field of all the AUTs is obtained by considering various SNR values in the decision threshold. The transformed pattern obtained using regular near-field data is compared with the transformed pattern using adaptive acquisition and the error level is computed as

$$\text{Error level} = 20\log_{10}\left(\left|\mathbf{E}_{\text{reg}}\left(\theta,\phi\right)\right| - \left|\mathbf{E}_{\text{adap}}\left(\theta,\phi\right)\right|\right). \tag{11}$$

Fig. 8 shows the transformed E-plane pattern cuts of the broad-beam antenna with lowest 20 dB SNR at maximum pattern level. As observed, good results have been obtained even with approx. 45% decrease in the number of measurement points. To clearly show the

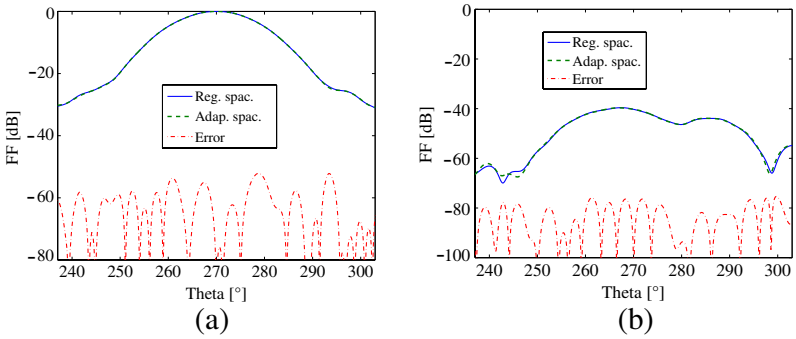

Figure 8. *E*-plane transformed far-field pattern cut ((a) co-pol and (b) cr-pol) using regular and adaptive processing of measured near-field data of broad-beam antenna.

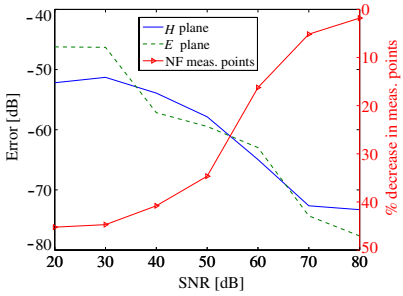

Figure 9. SNR at maximum pattern level versus maximum error level in the transformed *E*- and *H*-plane pattern cut of broad beam antenna (left *y*-axis) along with reduction in the number of measurement points (right *y*-axis).

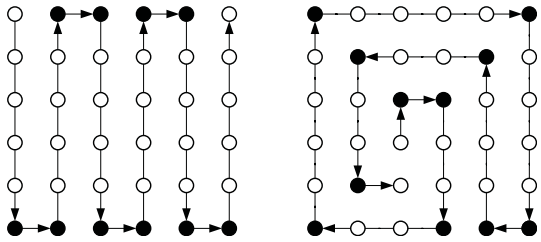

Figure 10. Traditional versus adaptive scanning technique (worst case). Black spots mark the position where the probe has to stop and change direction, thus causing an additional delay.

Table 1. Maximum error level in the valid region of transformed E- and H-plane pattern cuts with adaptive acquisition of near-field assuming 20 dB SNR at maximum pattern level.

AUT	Maximum Error Level [dB]			
	E-plane		H-plane	
	Co-pol.	Cr-pol.	Co-pol.	Cr-pol.
Medium gain	−67.3	−98.99	−64.77	−105.4
High gain	−68.18	−131.7	−67.17	−93.76
Broad-beam	−52.15	−75.36	−46.23	−68.42
Shaped-beam	−48.54	−65.8	−44.5	−58.8

effect of varying SNR in the decision threshold, maximum error in the transformed E- and H-plane pattern cut versus SNR at maximum pattern level is shown in Fig. 9. The percentage reduction in the number of measurement points is also shown on the right side of Fig. 9. As expected, accuracy of the transformed pattern increases by increasing the SNR value which in turn also increases the measurement points. Similar behavior is seen for all the antennas under test. The lowest accuracy at lowest SNR, i.e., 20 dB is tabulated in Table 1 for both E- and H-plane pattern cuts. The SNR can be increased for higher accuracy at the expense of more measurement points.

3.3. Data Acquisition Time

In a traditional measurement setup, the near-field is acquired by linear motion of the probe in vertical direction while stepping in the horizontal, or vice versa. Assuming the same scan speed v of the probe in the vertical and the horizontal direction, the total acquisition time t_{tot} can be expressed as

$$t_{\text{tot}} = \frac{L}{v} + Nt_{\text{mp}} + nt_{\text{delay}} \tag{12}$$

where L is the total length traversed by the probe in the vertical and the horizontal direction, N is the total number of measurement points, t_{mp} is the acquisition time at one measurement point, n is the number of times when the probe changes its direction while stepping, and t_{delay} represents the delay due to a single change. The black spots in Fig. 10 mark the position of the probe when it changes its direction.

The ring shaped adaptive data acquisition can be achieved by traversing the probe in a rectangular spiral locus while starting from the center of the scan plane and stepping in the outward direction

away from the center. The total acquisition time for the adaptive approach can also be expressed using Eq. (12) but with varying L and N according to the given decision threshold. The state-of-the-art RF equipment allows data acquisition by moving the probe in an on-the-fly manner due to negligible processing time at one single point. Therefore, one can neglect the term $(N\mathrm{t}_{\mathrm{mp}})$ from Eq. (12) as it is considerably less than that of the other two factors. The length L traversed by the probe in the traditional measurement can be calculated as $L_{\mathrm{trad}} =$ (length of one vertical column) (no. of vertical columns), whereas for the adaptive measurements it can be expressed as

$$L_{\mathrm{adap}} = \sum_{\mathbf{x}} \text{length of the ring } x$$

where $\mathbf{x}$ is a vector containing the number of the rings skipped during the measurement. Since all the rings have different lengths, the right knowledge of the skipped ring must be known for the correct length L. It is worth mentioning here that even if measurement is required at few points in one ring, it is assumed that the whole ring is measured for computing measurement time.

Table 2 summarizes the length traversed by the probe during traditional and adaptive measurements considering 20 dB SNR at maximum pattern level. Due to simplicity, we assume that the delay arising from changing the probe direction is the same for both cases, as can be seen from Fig. 10. However, less delay is expected in adaptive measurements if many measurement rings are skipped.

The efficiency in the measurement time is also shown in Table 2. As observed, best results have been achieved for the high gain antenna with smoothly varying near-field distribution while the worst case with zero efficiency is seen for the shaped beam antenna. The probe has to traverse the whole scan plane for the shaped beam antenna as not a

Table 2. Comparison between traditional and adaptive measurement in terms of number of measurement points and length L traversed by the probe assuming 20 dB SNR at maximum pattern level.

AUT	Meas. Points		Length L [m]		Meas. Time
	Tradi.	Adap.	Tradi.	Adap.	Efficiency
Medium gain	70756	36847	1068	655.45	38.63 %
High gain	34969	18329	131.6	69.94	46.85 %
Broad-beam	6889	3772	251	154.88	38.29 %
Shaped-beam	23345	16596	290	290	0.00 %

single ring can be skipped according to the given decision function. Nevertheless, no extra time is needed as compared to the traditional technique and since the whole scan plane is traversed one can utilize the whole near-field information for the maximum accuracy.

4. CONCLUSION

An adaptive planar near-field measurement technique is described to optimize the data acquisition time. The multilevel plane wave based near-field far-field transformation algorithm is used for the processing of the acquired near-field data. The multilevel approach gives the freedom of using irregular data with different sample spacing. Full probe correction and stability against measurement errors compared to traditional transformation algorithms are the major advantages of multilevel technique. The near-field data are acquired by traversing the probe in a rectangular spiral locus and obtaining the near-field in the form of rings. After covering a certain portion of the scan plane from the center, alternate rings of sampling points are measured and compared with already extrapolated values. A decision threshold based on the SNR of the acquired signal then determines whether the previous ring should be skipped or not. The proposed procedure is applied to both synthetic and real measurement data covering a variety of antennas. The acquisition time analysis showed that almost half of the measurement time can be saved for antennas with smoothly varying near-field distribution by using the proposed procedure and with a good accuracy. A worst case example with high fluctuations in the near-field region is also examined and simple computations showed no over-head time as compared to the traditional acquisition method.

ACKNOWLEDGMENT

The authors are grateful to D. J. van Rensburg and EADS Astrium for providing the near-field measurement data of the broad-beam and the shaped-beam antenna presented in Section 3.

REFERENCES

1. Hansen, J., *Spherical Near-field Antenna Measurements*, IEEE Electromagnetic Wave Series 26, UK, 1988.
2. Yaghjian, A. D., "Near-field antenna measurements on a cylindrical surface: A source scattering-matrix formulation," National Bureau of Standards, Tech. Note 696, Boulder, 1977.

3. Kerns, D., "Plane-wave scattering-matrix theory of antennas and antenna-antenna interactions," National Bureau of Standards, Boulder, CO, 1981.
4. Sarkar, T. K. and A. Taaghol, "Near-field to near-/far-field transformation for arbitrary near-field geometry utilizing an equivalent electric current and MoM," *IEEE Trans. Antennas Propag.*, Vol. 47, No. 3, 566–573, 2002.
5. Schmidt, C. H., M. M. Leibfritz, and T. F. Eibert, "Fully probe corrected near-field far-field transformation employing plane wave expansion and diagonal translation operators," *IEEE Trans. Antennas Propag.*, Vol. 56, No. 3, 737–746, 2008.
6. Yaghjian, A. D., "An overview of near-field antenna measurements," *IEEE Trans. Ant. Propag.*, Vol. 34, No. 1, 30–45, 1986.
7. Newell, A. C., "Error analysis techniques for planar near-field measurements," *IEEE Trans. Antennas Propag.*, Vol. 36, No. 6, 754–768, 1988.
8. Petre, P. and T. K. Sarkar, "Planar near-field to far-field transformation using an equivalent magnetic current approach," *IEEE Trans. Antennas Propag.*, Vol. 40, No. 11, 1348–1356, 1992.
9. Petre, P. and T. K. Sarkar, "Differences between modal expansion and intergral equation methods for planar near-field to far-field transformation," *Progress In Electromagnetics Research*, Vol. 12, 37–56, 1996.
10. Bucci, O. M. and M. D. Migliore, "A new method for avoiding the truncation error in near-field measurements," *IEEE Trans. Antennas Propag.*, Vol. 54, No. 10, 2940–2952, 2006.
11. Stark, H. and Y. Yang, *Vector Space Projections: A Numerical Approach to Signal and Image Processing, Neural Nets, and Optics*, Wiley-Interscience, 1988.
12. Martini, E., O. Breinbjerg, and S. Maci, "Reduction of truncation errors in planar near-field aperture antenna measurements using the Gerchberg-Papoulis algorithm," *IEEE Trans. Antennas Propag.*, Vol. 56, No. 11, 3485–3493, 2008.
13. Bucci, O. M., F. D'Agostino, C. Gennarelli, G. Riccio, and C. Savarese, "NF-FF transformation with plane-polar scanning: ellipsoidal modelling of the antenna," *Automatika*, Vol. 41, 159–164, 2000.
14. D'Agostino, F., F. Ferrara, C. Gennarelli, R. Guerriero, and M. Migliozzi, "An effective NF-FF transformation technique with planar spiral scanning tailored for quasi-planar antennas," *IEEE Trans. Antennas Propag.*, Vol. 56, No. 9, 2981–2987, 2008.

15. D'Agostino, F., F. Ferrara, C. Gennarelli, R. Guerriero, and G. Riccio, "An effective technique for reducing the truncation error in the near-field-far-field transformation with plane-polar scanning," *Progress In Electromagnetics Research*, Vol. 73, 213–238, 2007.
16. Ferrara, F., C. Gennarelli, R. Guerriero, G. Riccio, and C. Savarese, "An efficient near-field to far-field transformation using the planar widemesh scanning," *Journal of Electromagnetic Waves and Applications*, Vol. 21, No. 3, 341–357, 2007.
17. D'Agostino, F., F. Ferrara, C. Gennarelli, R. Guerriero, G. Riccio, and C. Savarese, "An efficient technique to lower the error due to the truncation of the scanning region in a bipolar facility," *Microwave and Optical Technology Letters*, Vol. 49, No. 12, 3033–3037, 2007.
18. Van Rensburg, D. J., D. McNamara, and G. Parsons, "Adaptive acquisition techniques for planar near-field antenna measurements," *33rd Annual AMTA Sympos.*, Denver, CO, 2011.
19. Qureshi, M. A., C. H. Schmidt, and T. F. Eibert, "Planar near-field measurement error analysis for multilevel plane wave based near-field far-field transformation," *33rd Annual AMTA Symposium*, Denver, CO, 2011.
20. Schmidt, C. H. and T. F. Eibert, "Multilevel plane wave based near-field far-field transformation for electrically large antennas in free-space or above material halfspace," *IEEE Trans. Antennas Propag.*, Vol. 57, No. 5, 1382–1390, 2009.
21. Newell, A. C. and M. L. Crawford, "Planar near-field measurements on high performance array antennas," National Bureau of Standards, NBSIR 74-380, 1974.
22. Yaghjian, A. D., "Upper-bound errors in far-field antenna parameters determined from planar near-field measurements, Part 1: Analysis," National Bureau of Standards, Tech. Note 667, 1975.
23. Coifman, R., V. Rokhlin, and S. Wandzura, "The fast multipole method for the wave-equation: A pedestrian prescription," *IEEE Antennas Propag. Mag.*, Vol. 35, No. 3, 7–12, 1993.
24. Saad, Y., *Iterative Methods for Sparse Linear Systems*, 2nd Edition, Society of Industrial and Applied Mathematics, 2003.
25. Schmidt, C. H., D. T. Schobert, and T. F. Eibert, "Electric dipole based synthetic data generation for probe-corrected near-field measurements," *5th European Conference on Antenna and Propagation*, Rome, Italy, 2011.